Advanced Steel Construction – Vol. 22 No. 3 (2026) 323–330
DOI:10.18057/IJASC.2026.22.3.8

FINITE ELEMENT ANALYSIS ON HYSTERETIC PERFORMANCE OF HOLLOW RIBBED HIGH-STRENGTH CONCRETE FILLED SQUARE STEEL TUBULAR COLUMNS

Ying Xie [1, *] and Xiao-Chuan Chen [2]

[1] *School of Civil Engineering and Architecture, Anhui Water Conservancy Technical College, Hefei 231603, China*
[2] *Anhui Provincial Key Laboratory of Building Earthquake Disaster Mitigation and Green Operations, Anhui Institute of Building Research & Design, Hefei 230088, China*
** (Corresponding author: E-mail: xiaochuan186@126.com)*

ABSTRACT

Hollow ribbed high-strength concrete filled square steel tubular columns offer several benefits, including lightweight, high load-bearing capacity, and ease of installation. Their internal hollow structure also facilitates the arrangement of pipelines in industrial and residential buildings, thereby saving space. This study aims to investigate the hysteretic behavior of these columns under cyclic loads using finite element analysis software, ABAQUS. Initially, the accuracy and applicability of the model established in this study are verified against existing literature. Subsequently, a comprehensive set of finite element models for hollow ribbed high-strength concrete filled square steel tubular columns are developed. These models undergo a full-process analysis, including stress analysis at various critical points. The study examines the influence of parameters such as steel ratio, yield strength of steel tubes, compressive strength of the concrete core, hollow ratio, and axial compression ratio on the hysteretic performance of the columns. Finally, the modified flexural capacity calculation equations are applied to the composite columns in this study and compared with the peak load from the skeleton curve. The findings reveal that the load-displacement curve of these columns can be categorized into three stages: elastic, elastic-plastic, and decline. During the elastic and plastic stages, the steel tubes primarily carry the load, while the internal ribs of the tubes delay member collapse in the decline stage. Based on the parameter analysis, it is recommended that the height of the stiffener should be limited to within 15% of the section width in design. The concrete strength is advised to be maintained below C90. The calculated flexural capacity aligns with the simulated values, with a mean error of 6.7%.

ARTICLE HISTORY

Received: 1 February 2025
Revised: 11 September 2025
Accepted: 20 September 2025

KEYWORDS

Hollow concrete filled square steel tube;
Stiffening rib;
Flexural bearing capacity;
Hysteresis performance;
Finite element analysis

1. Introduction

The construction industry's ongoing evolution, marked by a surge in large-scale projects like super-tall buildings, long-span structures, and bridges, has highlighted the critical need for research into the performance of structural components under complex loading scenarios, especially seismic forces. Concrete-filled steel tube (CFST) composite structures, representing an innovative approach in structural engineering, have found extensive application in high-rise construction and bridge projects. These structures leverage the strengths of both steel and concrete: the steel tube confers confinement on the core concrete, boosting its load-bearing capabilities, while the concrete inhibits local buckling of the steel tube. This collaborative interaction markedly enhances the structure's overall load-bearing capacity, ductility, and seismic resilience [1-3]. Furthermore, the hollow core of these structures streamlines the installation of pipelines in facilities such as factories and residential buildings, thereby optimizing space utilization. Consequently, this emerging composite structure, grounded in the CFST concept, presents a promising avenue for future structural design and application.

Scholars have conducted extensive research on the fundamental mechanical properties and seismic behavior of hollow CFST columns. Zhang et al[4] conducted numerical analyses using existing experimental data on hollow sandwich CFST columns, concluding that within the parameters of their study, the axial compressive capacity increased with rising concrete compressive strength, thicker inner steel tube walls, and decreasing length-to-diameter ratios and hollow ratios. Yang et al[5] determined the most appropriate concrete constitutive relationship model for hollow CFST short columns under axial compression. Li et al[6-7] developed a theoretical model for the skeleton curve and a calculation method for the displacement ductility coefficient based on quasi-static tests of hollow CFST columns. Ding et al[8] investigated the mechanical properties of circular hollow sandwich CFST superimposed columns under eccentric compression, finding that increasing the yield strength of the steel tube and the nominal steel ratio enhanced the specimen's eccentric compressive bearing capacity. Lu et al[9] researched hollow CFST columns under cyclic loading and established a more precise three-segment recovery force model. Li et al[10] compared the seismic performance of hollow sandwich CFST bridge piers with hollow concrete bridge piers through experimental results and finite element analysis. These studies collectively demonstrate the superior structural benefits and seismic performance of hollow CFST columns. However, they also reveal that when the outer steel tube is thin, it is prone to premature bulging. To mitigate this issue and enhance the steel tube's confinement effect on the concrete, welding stiffening ribs onto the outer steel tube wall is identified as an effective strategy for improving performance.

Several scholars have investigated the working mechanism of ribbed CFST columns under static and seismic loads. Li et al[11] conducted axial compression tests on 26 thin-walled square CFST short columns to examine their mechanical behavior. The findings indicated that stiffening ribs enhance the bearing capacity of the specimens and slow down the local bulging of the steel tube. An increase in the height of the stiffening ribs correspondingly raised the bearing capacity of the specimens and improved the stability of the steel tube wall. Xing et al[12] performed hysteretic tests on ribbed thin-walled square CFST columns, discovering that the stiffening ribs' constraint on the outer steel tube delayed the local bulging, thereby fully utilizing the material properties of the specimens. Wang et al[13] carried out quasi-static tests on ribbed cold-formed thin-walled square CFST columns, observing a significant improvement in the core concrete's strength due to the constraint of the ribbed cold-formed thin-walled square steel tube. Local buckling of the steel tube occurred post-peak load and was confined to the areas between the longitudinal stiffening ribs and the corners of the steel tube. Through parameter analysis, they developed a hysteretic model for this type of member.

In conclusion, research into the static and hysteretic behavior of both hollow and ribbed CFST columns has advanced significantly. Building on this foundation, the innovative structure of hollow ribbed high-strength concrete filled square steel tubular columns columns, which merges the benefits of both designs, has increasingly captured the attention of researchers. The hollow configuration not only reduces the structural weight but also enhances the steel tube's confinement effect on the core concrete through the ribbed design. This ribbed structure effectively constrains the transverse deformation of the concrete, slows down concrete cracking and failure, and improves the composite column's performance in terms of bearing capacity, deformation capacity, hysteretic behavior, and seismic resistance [14-15]. However, research on this structural form is still in its nascent stage, lacking comprehensive studies on its working mechanisms and hysteretic behavior. To ensure the seismic safety of buildings utilizing these members, it is imperative to conduct in-depth research on the seismic performance of hollow ribbed high-strength square CFST columns. This research will not only augment existing theories but also provide a crucial foundation for practical engineering design. This paper employs ABAQUS to numerically simulate the behavior of hollow ribbed high-strength concrete filled square steel tubular columns under cyclic loading. It analyzes the complete loading process of typical members and discusses the influence of various parameters, such as steel ratio, steel yield strength, and concrete compressive strength, on the seismic performance of the members.

2. Establishment of finite element models

2.1. Models design

A total of 12 finite element models of members were developed, with their specific parameters detailed in Table 1. A representative member, CFST-1, features a column length of 1200 mm, a square steel tube with a section width of 200 mm, an inner steel tube with an outer diameter of 80 mm, and both the outer and inner steel tubes have a wall thickness of 5 mm. The steel's yield strength is 690 MPa, and the compressive strength of the concrete within the tube column is 80 MPa. Rib plates are welded to the middle position of the outer steel tube's web, measuring 30 mm in height, 10 mm in thickness, and with a yield strength of 690 MPa. The cross-section of this member is depicted in Fig. 1.

Table 1
Model details

Model No	$B\times t_1\times t_2\times L$/mm	F_{y1}/MPa	F_{y2}/MPa	f_{cu}/MPa	h	n
CFST-1	200×5×3×1200	690	690	80	30	0.3
CFST-2	200×5×3×1200	690	690	80	10	0.3
CFST-3	200×5×3×1200	690	690	80	20	0.3
CFST-4	200×5×3×1200	690	690	80	40	0.3
CFST-5	200×5×3×1200	690	690	80	50	0.3
CFST-6	200×5×3×1200	460	460	80	30	0.3
CFST-7	200×5×3×1200	770	770	80	30	0.3
CFST-8	200×5×3×1200	890	890	80	30	0.3
CFST-9	200×5×3×1200	690	690	60	30	0.3
CFST-10	200×5×3×1200	690	690	70	30	0.3
CFST-11	200×5×3×1200	690	690	90	30	0.3
CFST-12	200×5×3×1200	690	690	100	30	0.3

Note：B is the column width, t_1 is the outer steel tube thickness, t_2 is the inner steel tube thickness, L is the column height, f_y is the steel yield strength ；$f_{cu}$is the concrete compressive strength, h is the rib height, n is the axial compression ratio.

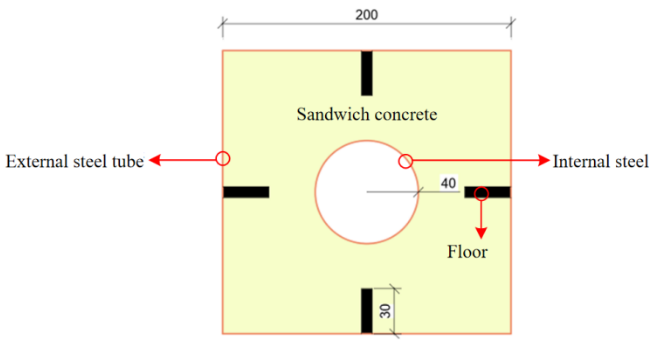

Fig. 1 Cross section design(mm)

2.2. Element types and boundary conditions

Concrete, steel tubes, rib plates, and cover plates were all represented using three-dimensional solid elements with reduced integration and eight nodes (C3D8R). The meshing and boundary conditions are illustrated in Fig. 2. The contact relationships between the components were defined as follows: the cover plate and the inner and outer steel tubes employed "tie" contact, same for the outer steel tube and the rib plates. The cover plate and the concrete utilized a "hard contact". The normal direction between the steel tube and the sandwich concrete, as well as between the rib plates and the concrete, was set to "hard contact". The tangential direction employed the Coulomb friction model with a friction coefficient of 0.6[16].

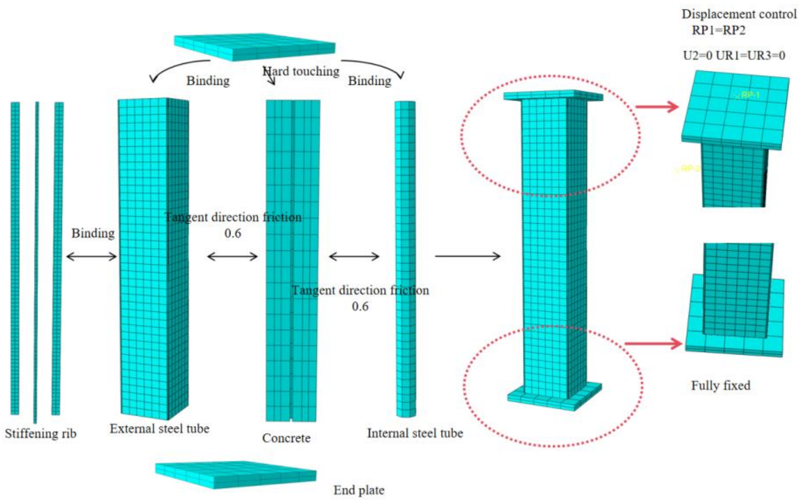

Fig. 2 Boundary conditions

2.3. Constitutive models

In the ABAQUS simulation, the concrete's behavior was modeled using the concrete plasticity damage(CDP) model to capture its constitutive relationship. The stress-strain relationship for the core concrete, which accounts for the confining effect of the steel tube, was based on the model proposed by Liu[17]. The high-strength steel material was represented using a bilinear model [18].

2.4. Model verification

To validate the accuracy of the finite element modeling approach, the method outlined above was applied to model and analyze specimens from literature[19-20]. A comparison of the finite element simulation results with the experimental data from the literature is presented in Fig. 3. The comparison shows that the error in bearing capacity between the finite element and experimental results is within 5%, and the overall curves align closely.

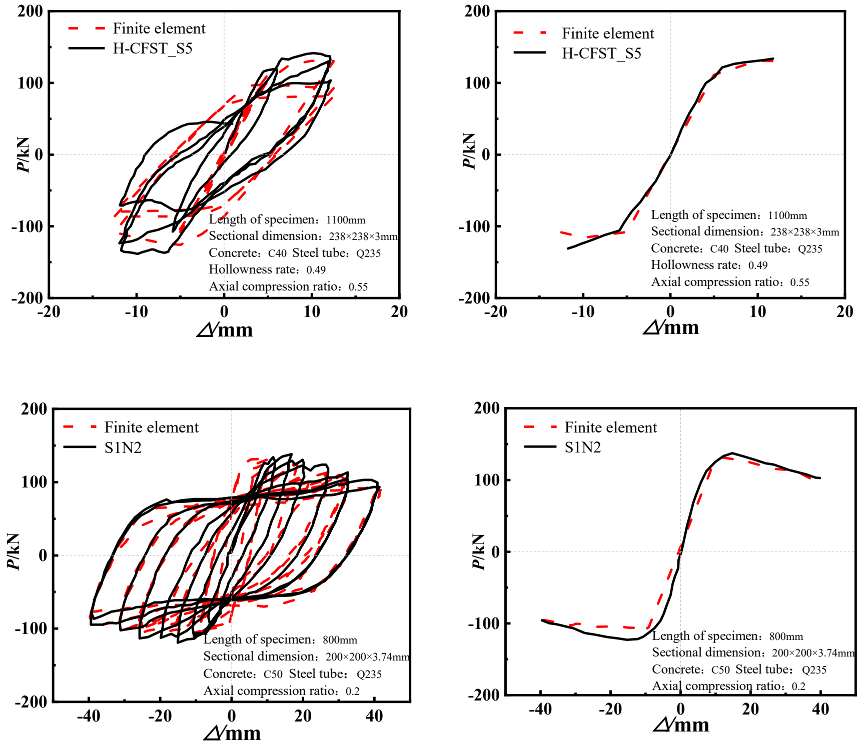

Fig. 3 Model verification

3. Full stress process analysis of typical member

To investigate the seismic performance of hollow ribbed high-strength concrete filled square steel tubular columns, a comprehensive force analysis was carried out on the selected typical member CFST-1.

3.1. Stress process

The load-displacement skeleton curve for the typical member CFST-1 is depicted in Fig. 4. This curve can be categorized into three distinct stages:

Elastic Stage (OA): During the initial loading phase, both the concrete and the steel tubes, both inner and outer, as well as the rib plates, remain in the elastic state. As the horizontal displacement increases, the horizontal load does so linearly, maintaining a constant slope, indicative of a rapid load increase with displacement. The member exhibits a high initial stiffness. In this elastic stage, the stress in the outer steel tube exceeds that in the inner tube, with the stiffening ribs sharing a larger portion of the stress along with the outer tube. At point A, the member's load capacity reaches 87.3% of the peak load, and the outer steel tube in the compression zone is on the verge of yielding.

Elastoplastic Stage (AB): In this stage, the curve continues to ascend. As plastic deformation occurs in the outer steel tube, rib plates, and concrete, the member's stiffness starts to diminish, resulting in a decreasing slope of the curve. The member undergoes overall plastic deformation, transitioning from the elastic to the plastic stage, characterized by a nonlinear relationship between load and displacement. The steel tube's constraint effect on the concrete is significantly enhanced. At point B, the member attains its peak load capacity of 434.2 kN, with the peak displacement being 32.16 mm.

Decline Stage (BC): Beyond the peak point B, the stress in the inner steel tube gradually intensifies and reaches yielding, with the member predominantly in the plastic stage. The load decreases as displacement increases. Following the peak load, the member's load capacity continues to diminish with increasing displacement, accompanied by pronounced bulging of the steel tube. The member is deemed destroyed when the load reaches 85% of the peak load [21].

3.2. Stress analysis

Fig. 5 illustrates the Mises stress for both the inner and outer steel tubes, the stiffening ribs, and the S33 stress of the concrete at the corresponding feature points of the typical member CFST-1.

(1) Feature Point A: At yield point A, the stress in the outer steel tube at the column base approaches the yield stress at approximately 680.1 MPa, while the stress in the inner steel tube remains relatively low at 420.4 MPa. The stiffening ribs deform in tandem with the outer steel tube, reaching a stress of 684.2 MPa, which underscores their effectiveness. During the initial loading phase, the majority of the concrete is under compression, exhibiting a longitudinal stress of $0.03f_c$ on the tensile side and $1.02f_c$ on the compressive side. This indicates that the steel tube provides confinement to the sandwich concrete.

(2) Feature Point B: At the peak point B, both the outer steel tube and the stiffening ribs have yielded, with the yielded area progressively expanding. However, the stress in the steel tube increases slowly, and the stiffening ribs delay the bulging of the tube. The stress in the inner steel tube also rises, reaching 588.1 MPa at point B. The longitudinal stress on the tensile side of the sandwiched concrete is $0.85f_c$, and on the compressive side, it is $1.55f_c$, suggesting that the confinement effect of the steel tube on the concrete intensifies with increasing load.

(3) Feature Point C: At the ultimate point C, the tensile and compressive zones of the outer steel tube start to merge, causing the deformation to reach its maximum and resulting in the failure of the steel tube. The longitudinal stress on the tensile side of the sandwiched concrete is $0.14f_c$, and on the compressive side, it is $1.85f_c$. Owing to the confinement provided by the inner and outer steel tubes and the rib plates, the concrete demonstrates a higher bearing capacity. The deformation of the rib plates is primarily concentrated at the base of the column, corresponding to the bulging position of the steel tube and the crushing position of the concrete. The inner steel tube yields, reaching 742.7 MPa, and the maximum stress at the base of the column for the outer steel tube and rib plate is 754.8 MPa, achieving the ultimate tensile strength.

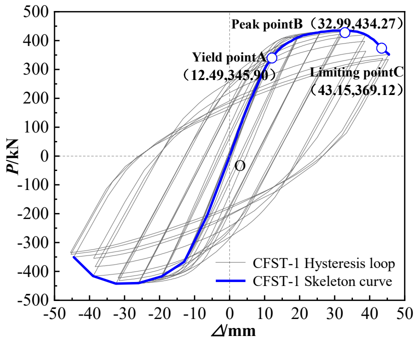

Fig. 4 load-displacement skeleton curve of typical member

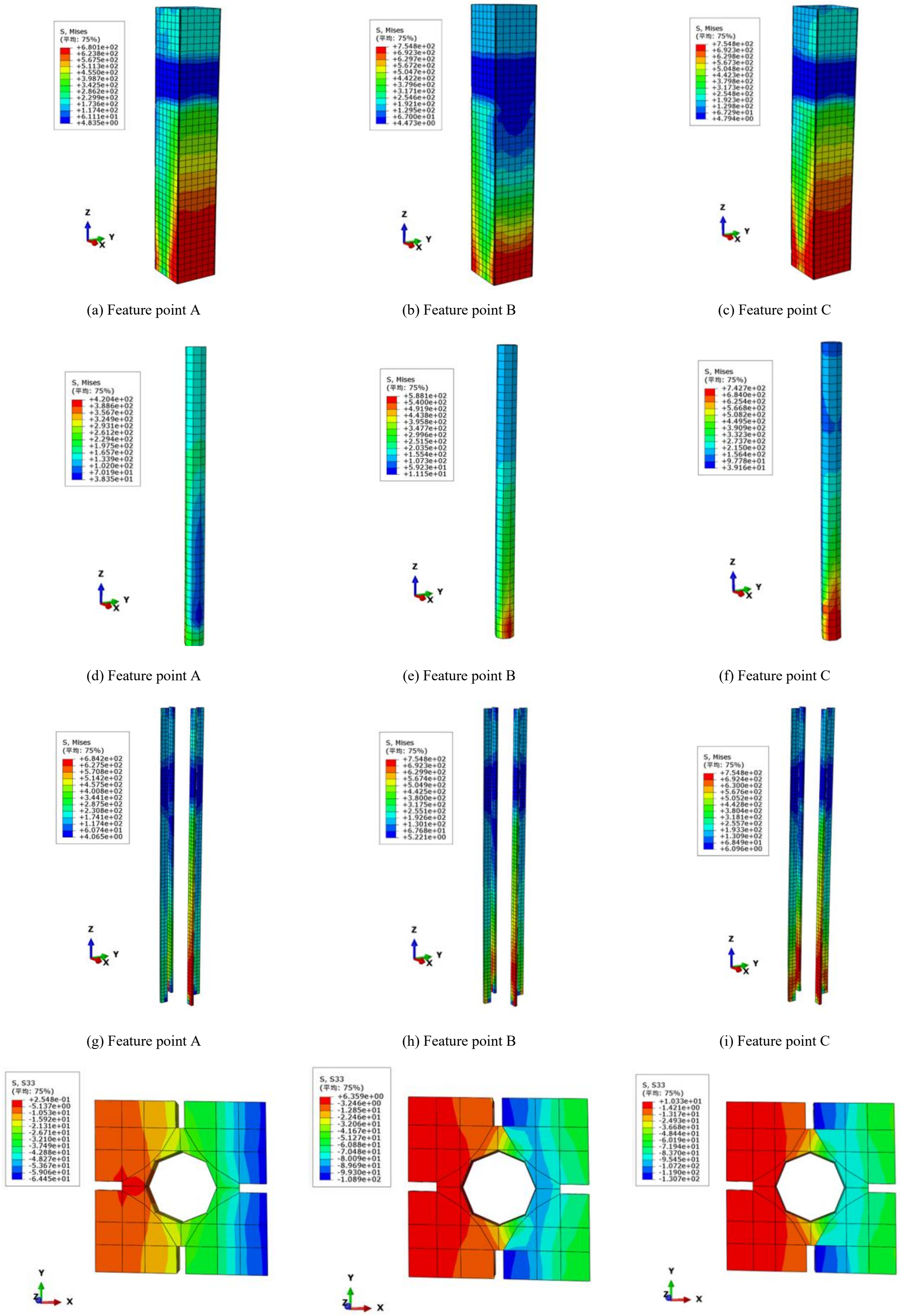

(a) Feature point A (b) Feature point B (c) Feature point C

(d) Feature point A (e) Feature point B (f) Feature point C

(g) Feature point A (h) Feature point B (i) Feature point C

(j) Feature point A (k) Feature point B (l) Feature point C

Fig. 5 Stress distribution of components

4. Parameter analysis

The effects of steel ratio (height of stiffening ribs), yield strength of steel tubes, and compressive strength of concrete on the seismic behavior of the members were analyzed.

4.1. Hysteresis curves

Fig. 6 presents the hysteresis curves for each member. As observed in the figure, the hysteresis curves predominantly exhibit a diamond shape, which becomes more filled as the displacement increases. The steel ratio and yield strength of the steel tubes notably influence the shape of the hysteresis curves. The “pinching” phenomenon is generally not pronounced in most of the hysteresis curves, with only a slight occurrence in the hysteresis curve of member CFST-6, where the yield strength of the steel tube is 460 MPa. This suggests that the hollow ribbed high-strength square steel tube concrete columns possess favorable seismic performance. In the initial loading stage, the area enclosed by the hysteresis loops is small, with no significant residual deformation, and the steel ratio of the member is minimal. As the displacement increases, the area enclosed by the hysteresis loops gradually increases, and the energy-dissipation of the member also increases correspondingly.

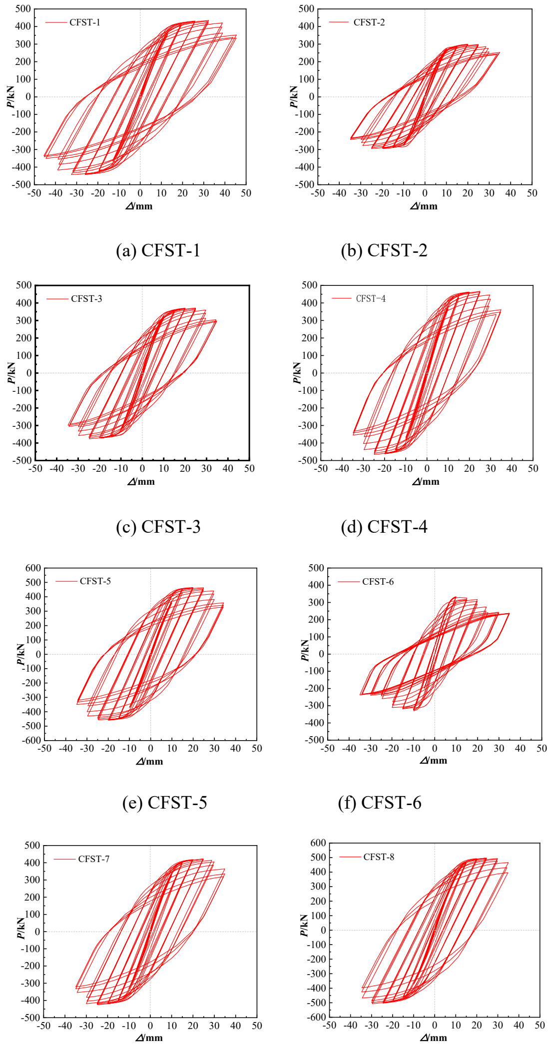

(a) CFST-1 (b) CFST-2

(c) CFST-3 (d) CFST-4

(e) CFST-5 (f) CFST-6

(g) CFST-7 (h) CFST-8

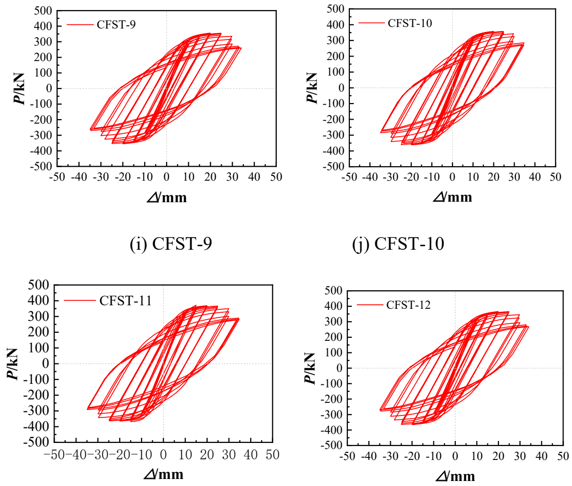

(i) CFST-9 (j) CFST-10

(k) CFST-11 (l) CFST-12

Fig. 6 Hysteresis curves with different parameters

4.2. Skeleton curves

Fig. 7 depicts the influence of parameter variations on the skeleton curves. Fig. 7(a) demonstrates the impact of different steel ratios. It is evident that with an increase in the steel ratio, the initial stiffness of the member progressively enhances, the elastic stage extends, the yield displacement rises, and the peak bearing capacity improves, while the overall shape of the skeleton curve remains largely consistent. For every 1% increase in the steel ratio, that is, for each 10 mm increase in the height of the stiffening ribs from 10 mm to 50 mm, the peak bearing capacity of the member increases by 20.1%, 11.5%, 5.9%, and 3.4%, respectively. This indicates that augmenting the steel ratio can effectively boost the peak bearing capacity of the member, with the most substantial enhancement occurring.

Fig. 7(b) displays the skeleton curves for various yield strengths of the steel tubes. It is apparent that as the yield strength of the steel tubes rises, the elastic stages of the members with different parameters remain largely unchanged, the peak bearing capacity increases, and the descending segment becomes steeper. When the yield strength of the steel tubes is elevated from 460 MPa to 890 MPa, the peak bearing capacity of the members increases by 11.2%, 7.8%, and 5.8%, respectively.

Fig. 7(c) presents the skeleton curves for different compressive strengths of the concrete. It is noticeable that changes in the compressive strength of the concrete have a relatively modest impact on the overall skeleton curve compared to the previous two parameter alterations. There is no substantial difference in the initial stiffness of the members. When the compressive strength of the concrete is raised from 60 MPa to 100 MPa, the peak bearing capacity of the members increases by 3.3%, 1.2%, 2.5%, and 0.6%, respectively.

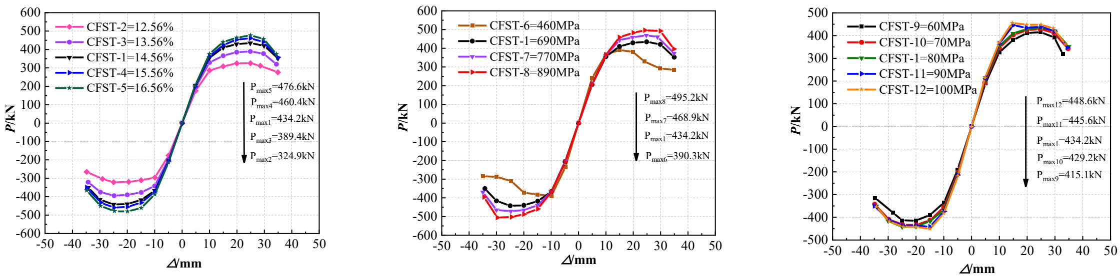

(a) Steel ratio (b) Steel yield strength (c) Concrete compressive strength

Fig. 7 Skeleton curves with different parameters

4.3. Ductility coefficient

The ductility of the members is determined using the displacement ductility coefficient μ, which is calculated according to Eq. (1) [22].

$$\mu = \frac{|\Delta_u^+| + |\Delta_u^-|}{|\Delta_y^+| + |\Delta_y^-|} \tag{1}$$

In which, Δ^+_y and Δ^+_u are positive yield and ultimate displacement, Δ^-_y、Δ^-_u are negative yield and ultimate displacement.The ultimate displacement is the horizontal displacement corresponding to the point where the peak load decreases to 85% of its value; the yield displacement is determined using the equivalent energy method.

Fig. 8 provides insights into how changes in specific parameters affect the skeleton curves of the members. Fig. 8(a) highlights the influence of varying steel ratios. It is evident that an increase in the steel ratio leads to a gradual enhancement of the member's initial stiffness, an extension of the elastic stage, an increase in yield displacement, and an improvement in peak bearing capacity, while the fundamental shape of the skeleton curve remains largely unchanged. For each 1% increase in the steel ratio, corresponding to a 10 mm increase in the height of the stiffening ribs from 10 mm to 50 mm, the peak bearing capacity of the member increases by 20.1%, 11.5%, 5.9%, and 3.4%, respectively. This indicates that increasing the steel ratio can significantly enhance the peak bearing capacity of the member, with the most substantial improvement observed. Fig. 8(b) illustrates the skeleton curves for different yield strengths of the steel tubes. It can be observed that as the yield strength of the steel tubes increases, the elastic stages of the members with different parameters remain largely consistent, while the peak bearing capacity improves and the descending segment becomes steeper. When the yield strength of the steel tubes is increased from 460 MPa to 890 MPa, the peak bearing capacity of the members increases by 11.2%, 7.8%, and 5.8%, respectively. Fig. 8(c) shows the skeleton curves for various compressive strengths of the concrete. It is evident that changes in the compressive strength of the concrete have a relatively smaller impact on the overall skeleton curve compared to the previous two parameter changes. There is no significant difference in the initial stiffness of the members. When the compressive strength of the concrete is increased from 60 MPa to 100 MPa, the peak bearing capacity of the members increases by 3.3%, 1.2%, 2.5%, and 0.6%, respectively.

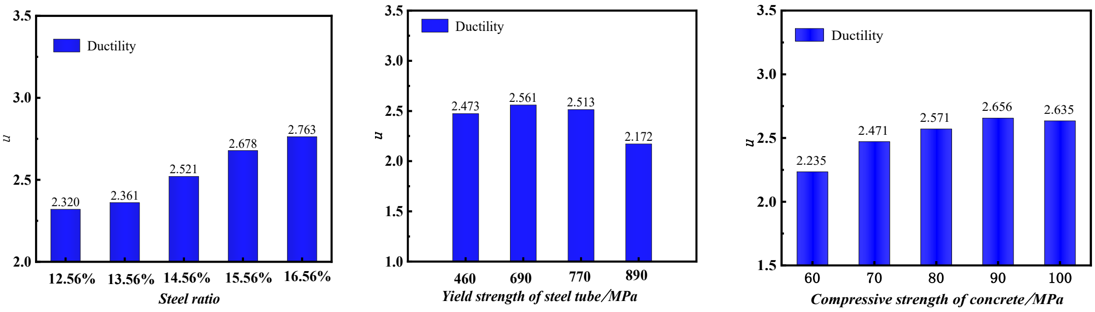

(a) Steel ratio (b) Steel yield strength (c) Concrete compressive strength

Fig. 8 Ductility coefficient with different parameters

4.4. Stiffness degradation

The stiffness degradation of the members is represented by the secant stiffness Ki, which is calculated according to Eq. (2) [23-24].

$$K_i = \frac{|+P_i| + |-P_i|}{|+\Delta_i| + |-\Delta_i|} \tag{2}$$

In which, P_i is the peak load of the first cycle at the i-th control displacement; Δ_i is the displacement value corresponding to the peak load.

Fig. 9 depicts the influence of parameter changes on the stiffness degradation of the members. In Fig. 9(a), the stiffness degradation curves are presented for different steel ratios. It is evident that a lower steel ratio, which corresponds to a smaller height of the stiffening ribs, results in a relatively faster stiffness degradation rate. As the members approach destruction, the stiffness degradation rates for members with rib heights of 10, 20, 30, 40, and 50 mm are found to be 80.2%, 79.1%, 77.3%, 75.4%, and 76.3%, respectively. Notably, the member with a steel ratio of 12.56% and a rib height of 10 mm exhibits the most significant stiffness degradation. This observation suggests that increasing the steel ratio can effectively enhance the initial stiffness of the member. Fig. 9(b) illustrates the impact of varying yield strengths of the steel tubes on the stiffness degradation curves of the members. It is observed that the yield strength of the steel tubes has a relatively minor effect on the initial stiffness. The stiffness degradation rates for the members are 84.2%, 77.3%, 75.4%, and 75.6%, respectively, indicating that the stiffness degradation is most pronounced when the yield strength is 460 MPa. Fig. 9(c) displays the effect of concrete compressive strength on the stiffness degradation of the members. It is apparent that as the concrete compressive strength increases, the initial stiffness of the members is greater. However, the overall impact of concrete compressive strength on stiffness degradation is not significant.

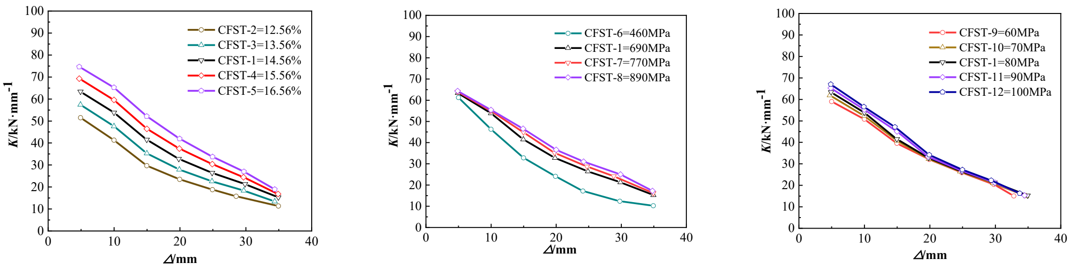

(a) Steel ratio (b) Steel yield strength (c) Concrete compressive strength

Fig. 9 Stiffness degradation with different parameters

4.5. Energy-dissipation capacity

The energy-dissipation capacity of the members is calculated as the area enclosed by the hysteresis loop in one cycle of the hysteresis curve, and is represented by the energy-dissipation coefficient E, which is calculated according to Eq. (3) [25-26].

$$E = \frac{S_{ABCDA}}{S_{\Delta OAE} + S_{\Delta OCF}} \tag{3}$$

In which, S_{ABCDA} is the area enclosed by the hysteresis curve; $S_{\triangle OAE}$ and $S_{\triangle OCF}$ are as shown in Fig. 10.

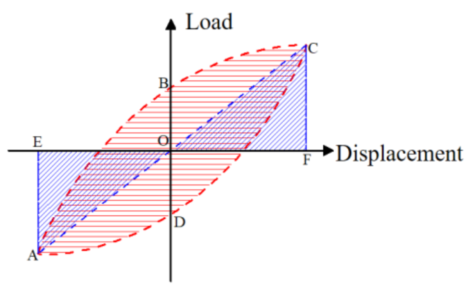

Fig.10 Energy-dissipation calculation

Fig. 11 highlights the influence of parameter changes on the energy-dissipation capacity of the members. In Fig. 11(a), the effect of different steel ratios on the energy-dissipation capacity is illustrated. It is evident that a higher steel ratio correlates with a stronger energy-dissipation capacity for the members. As the steel ratio increases from 12.56% to 16.56%, the cumulative energy-dissipation of the members ultimately rises by 33.1%. Notably, the member with a rib height of 50 mm exhibits the strongest energy-dissipation capacity. Fig. 11(b) presents the energy-dissipation curves for different steel tube yield strengths. The member with a yield strength of 460 MPa demonstrates a superior initial energy-dissipation capacity, which tends to weaken gradually during the loading process. The general trend observed is that the higher the yield strength, the greater the energy-dissipation capacity of the member. Fig. 11(c) shows the influence of concrete compressive strength on the energy-dissipation capacity of the members. As depicted in the figure, variations in concrete compressive strength have a minimal effect on the energy-dissipation capacity of the members, with the energy-dissipation curves being largely overlapping.

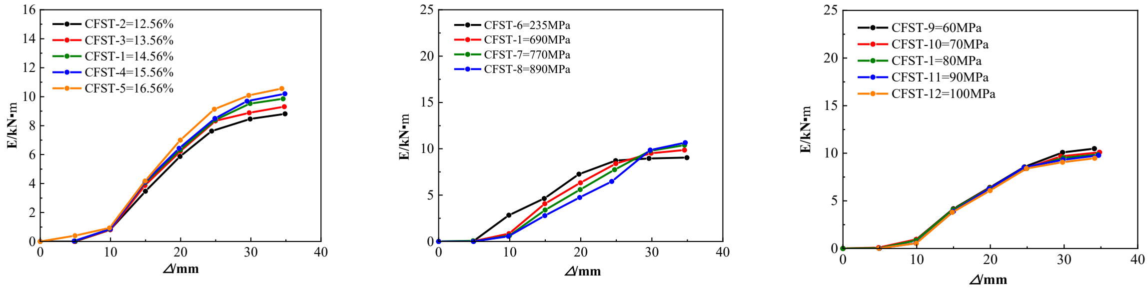

(a) Steel ratio (b) Steel yield strength (c) Concrete compressive strength

Fig. 11 Energy-dissipation capacity with different parameters

5. Flexural capacity calculation

To determine the flexural bearing capacity of hollow ribbed high-strength concrete filled square steel tubular columns under monotonic loading, this paper adapts and applies the simplified calculation method for the flexural bearing capacity of hollow CFST members as outlined in the T/CCES 7-2020 code[27], along with the calculation method proposed by Professor Han Linhai for the flexural bearing capacity of ribbed concrete filled square steel tubular columns [2]. The modified calculation equations for the flexural bearing capacity of the composite columns in this study is as follows:

$$\frac{1}{\varphi}\bullet\frac{N}{N_u}+\frac{a}{b}\bullet\frac{M}{M_u}=1 \qquad \left(\frac{N}{N_u}\geq 2\varphi^3\eta_0\right) \tag{4}$$

$$-b\bullet\left(\frac{N}{N_u}\right)^2-c\bullet\frac{N}{N_u}+\frac{1}{d}\bullet\frac{M}{M_u}=1 \qquad \left(\frac{N}{N_u}<2\varphi^3\eta_0\right) \tag{5}$$

$$N_{osc,u}=f_{osc}\left(A_{so}+A_c\right) \tag{6}$$

$$f_{osc}=C_1\chi^2 f_{yo}+C_2\left(1.14+1.02\xi\right)f_{ck} \tag{7}$$

$$N_{i,u}=f_{yi}A_{si} \tag{8}$$

In which, N_u and M_u are axial compressive and bending capacity of the member. $N_{osc,u}$ and $N_{i,u}$ are strength of outer and inner steel tube cross sections. A_c, A_{si} and A_{so} are cross section area of concrete, inner and outer steel tube. C1 and C2 are steel ratio coefficients. ξ is the confinement coefficient of sandwich concrete. f_{ck}, f_{yi} and f_{yo} are strength of sandwich concrete, inner and outer steel. The indexes a, b, c, d and φ are determined according to references [2] and [27]. η_0 is determined according to Eq. (9)-(10). The bending capacity M_u is determined according to Eq. (11).

$$\eta_0=\left(0.5-0.245\xi\right)\bullet\left(1+0.7\chi-1.8\chi^2\right) \qquad \left(\xi\leq 0.4\right) \tag{9}$$

$$\eta_0=\left(0.1+0.14\xi^{-0.84}\right)\bullet\left(1+0.7\chi-1.8\chi^2\right) \qquad \left(\xi>0.4\right) \tag{10}$$

$$M_u=\gamma_{m1}W_{scm}f_{osc}+\gamma_{m2}W_{si}f_{yi}+W_1 f_y \tag{11}$$

$$\gamma_{m1}=1.1+0.48\ln\left(\xi+0.1\right)\left(1+0.06\chi-0.85\chi^2\right) \tag{12}$$

$$\gamma_{m2}=1.04\chi^{-0.67}-0.02\chi^{-2.76}\ln\xi \tag{13}$$

In which, W_{scm} and W_{si} are the section flexural modulus of outer steel tube and inner steel tube and concrete respectively. f_y is the yield strength of ribs. W_1 is the section resistance moment of the stiffened plate.

Utilizing the aforementioned calculation method, the flexural bearing capacity of hollow ribbed high-strength concrete filled square steel tubular columns under monotonic loading were computed in this paper. The calculated flexural bearing capacity of the members were then compared with the peak loads obtained from the simulated skeleton curves, as detailed in Table 2 and illustrated in Fig. 12. The error values for the specimens all fall below 10%, with an average error of 6.7% and a variance of 2.1%. This indicates that the discrepancy between the calculated values and the simulated values is relatively small, suggesting that this calculation formula is suitable for determining the flexural bearing capacity of hollow ribbed high-strength concrete filled square steel tubular columns.

Table 2
Comparison of calculated and simulated values

Model No.	$P_{max,s}$(kN)	$P_{max,c}$(kN)	Error(%)
CFST-1	434.2	405.2	6.7
CFST-2	324.9	340.6	4.8
CFST-3	389.4	368.1	5.5
CFST-4	460.4	435.6	5.4
CFST-5	476.6	451.3	5.3
CFST-6	390.3	420.1	7.6
CFST-7	468.9	441.5	5.8
CFST-8	495.2	452.8	8.6
CFST-9	415.1	377.3	9.1
CFST-10	429.2	392.3	8.6
CFST-11	445.6	421.1	5.5
CFST-12	448.6	416.9	7.1
Average	-		6.7
Variance	-		2.1

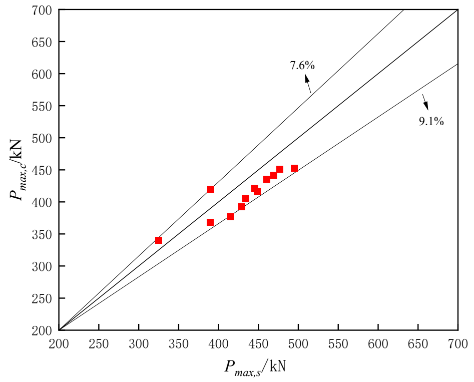

Fig. 12 Comparison of calculated and simulated flexural capacity

6. Conclusions

In this paper, a novel hollow ribbed high-strength concrete filled square steel tubular column is introduced, and the working mechanism as well as the function of the stiffening rib are elucidated. The study investigates the impact of variations in the height of the stiffening rib, the yield strength of the steel tube, and the concrete strength parameters on the hysteretic performance of the member, offering design recommendations. Equations for calculating the flexural bearing capacity suitable for this member is also proposed. The specific conclusions are as follows:

(1) The load-displacement behavior of hollow ribbed high-strength concrete filled square steel tubular columns can be categorized into 3 distinct stages: the elastic stage, the elastic-plastic stage, and the decline stage. During the elastic stage, the load is primarily borne by the steel tube. In the elastic-plastic stage, the steel tube's constraint on the concrete significantly intensifies. In the decline stage, the internal rib plate becomes active, enhancing the member's ductility, delaying the steel tube's bulging, and further reinforcing the steel tube's constraint on the concrete.

(2) Considering parameters such as bearing capacity, stiffness degradation, and energy dissipation capacity, it is advisable to design the member with a stiffening rib height that is within 15% of the section width. The yield strength of the steel tube is recommended to be in the range of 460MPa to 770MPa. Additionally, it is suggested to use concrete with a grade below C90, as higher-grade concrete does not significantly enhance the bearing capacity and may decrease ductility.

(3) In this paper, the proposed calculation method for the flexural bearing capacity of hollow ribbed high-strength concrete filled square steel tubular columns is utilized to determine the flexural bearing capacity of the composite columns. The calculation results show a high degree of consistency, with an average error of 6.7% and a mean square error of 2.1%.

Funding

The research was funded by the Anhui Provincial Natural Science Foundation(2022AHO52286), Open Research Fund of Anhui Provincial Key Laboratory of Building Earthquake Disaster Mitigation and Green Operations(2022-JKYL-001).

References

[1] Zhong ST. concrete filled steel tubular structure[M]. Beijing: Tsinghua University press. 2003 (in Chinese).
[2] Liu X, Huang DD, Hou XY, et al, The bond behavior of the interface between high-strength concrete-filled double-skin steel tube[J], Journal of Constructional Steel Research, 2025, 226, 109320.
[3] Liu YJ, Sun LP, Zhou XH, et al. Progress in the application of research on concrete-filled steel tubular bridge towers[J]. China Journal of Highway and Transport, 2022, 35(06): 1-21 (in Chinese).
[4] Zhang XY, Gao ZY, Bai PK, et al. Finite element analysis of axial compression performance of concrete-filled double skin steel tube[J]. Concrete, 2024, (04): 115-121 (in Chinese).
[5] Yang ZJ, Zuo WZ. Finite Element Analysis on Axial Compressive Performance of RHHCFST Short Columns with Longitudinal Stiffeners[J]. Steel Construction(Chinese & English), 2024, 39(07): 19-28 (in Chinese).
[6] Zha XX. Hollow and solid concrete filled steel tubular structures[M]. Beijing: science press. 2011 (in Chinese).
[7] Li WQ, Zha XX, Yu M. Seismic behavior study of hollow ordinary concrete and recycled aggregate concrete filled steel tubular(CFST) columns I: experimental and FEM study[J]. Progress in Steel Building Structures, 2012, 14(03): 27-35 (in Chinese).
[8] Ding JN, Ren QX, Wang QH, et al. Mechanical Performance of Circular Concrete-encased CFDST Columns under Eccentric Compression[J]. Journal of Shenyang Jianzhu University(Natural Science), 2023, 39(03): 411-419 (in Chinese).
[9] Lu DH, Wang HW, Zhou Y. Research on Resilience Formula of Hollow Concrete-filled Steel Tube Based on OpenSees[J]. Journal of Disaster Prevention and Mitigation Engineering, 2014, 34(05): 626-631 (in Chinese).
[10] Li Z, Du C, Liu D, et al. Comparative study on seismic performance of concrete-filled double skin tubular piers and hollow concrete piers: experimental and analytical[J]. Structures, 2023, 49: 1078-92.
[11] Li B, Guo SZ, Gao CY. Experimental research on mechanics behavior of stub-column concrete-filled thin-walled stiffened square steel tube under axial load[J]. Concrete, 2018, (03): 53-55+59 (in Chinese).
[12] Xing X, Li B, Gao CY. Research on the seismic behavior of concrete filled thin-walled stiffened square steel tubular columns[J]. Progress in Steel Building Structures, 2021, 23(09): 25-31 (in Chinese).
[13] Wang ZB, Guo JT, Zhang WA, et al. Hysteretic behaviour of concrete-filled square cold-formed thin-walled steel tubular beam-columns with longitudinal stiffeners[J]. Journal of Building Structures, 2019, 40(11): 172-181 (in Chinese).
[14] Cao HL, Li HF, Jiang AL, et al. Seismic behavior of box steel pier embedded energy-dissipation steel plates with stiffeners[J/OL]. Building Structure, 1-11[2024-10-14] (in Chinese).
[15] Xiao C, Lv H, Luo J. Seismic energy dissipation analysis of concrete-filled square steel tubular columns with stiffeners at column ends[J]. Earthquake Resistant Engineering and Retrofitting, 2024, 46(02): 121-129 (in Chinese).
[16] HAN L H, YAO G H, TAO Z. Performance of concrete-filled thin-walled steel tubes under pure torsion[J]. Thin-Walled Structures, 2007, 45(1): 24-36.
[17] Liu W. Research on mechanism of concrete-filled steel tubes subjected to local compression[D]. Fuzhou: Fuzhou University, 2006 (in Chinese).
[18] Khan M, Uy B, Tao Z, et al. Concentrically loaded slender square hollow and composite columns incorporating high strength properties[J]. Engineering Structures, 2017, 131: 69-89.
[19] Wang HW, Lu DH, Zhou Y. Experimental study on seismic behavior of hollow concrete-filled steel tubes(H-CFST) under low cyclic loading[J]. Earthquake Engineering and Engineering Dynamics, 2014, 34(2): 129-136 (in Chinese).
[20] Jing CG. Mechanism and design method of reinforced concrete filled square steel tubular columns[D]. Nanning: Nanning University, 2023 (in Chinese).
[21] Research group on seismic behavior of members subjected to axial load, bending and shear. Experimental research on seismic behavior of reinforced concrete member subjected to axial load, bending and shear[J]. Journal of Building Structures, 1992, 2: 2-10 (in Chinese).
[22] Chen ZH, Dong SS, Du YS. Experimental study and numerical analysis on seismic performance of FRP confined high-strength rectangular concrete-filled steel tube columns[J]. Thin-Walled structures, 2021, 162(5), 107560.
[23] Zhang Y, Xu C, Lu X. Experimental study of hysteretic behaviour for concrete-filled square thin-walled steel tubular columns[J]. Journal of Constructional Steel Research, 2007, 63(3): 317-325.
[24] Zheng W, Ji J. Dynamic performance of angle-steel concrete columns under low cyclic loading-I: Experimental study[J]. Earthquake Engineering and Engineering Vibration, 2008, 7(1): 67-75.
[25] Chen ZX, Hu HS, Xu L, et al. Experimental study on seismic behavior of square spiral-confined ultra-high-strength concrete-filled steel tube columns[J]. Journal of Building Structures, 2021, 42(S2): 288-294 (in Chinese).
[26] Fang C, Zhou F, Wu ZY, et al. Concrete-filled elliptical hollow section beam-columns under seismic loading [J]. Journal of Structural Engineering, 2020, 146(8), 4020144.
[27] T/CCES 7-2020. Technical specification for concrete-filled double skin steel tube structure[S]. Beijing: China building industry press. 2020 (in Chinese).